SEHS: Simultaneous Energy Harvesting and Sensing using Piezoelectric Energy Harvester

Dong Ma*‡, Guohao Lan*‡, Weitao Xu*†, Mahbub Hassan*‡, and Wen Hu*‡
*University of New South Wales, † Shenzhen University, ‡Data61 CSIRO
dong.ma1@student.unsw.edu.au*, weitao.xu@szu.edu.cn†
{guohao.lan, mahbub.hassan, wen.hu}@unsw.edu.au*

***Abstract*—Piezoelectric energy harvesting (PEH), which converts ambient motion, stress, and vibrations into usable electricity, may help combat battery issues in a growing number of industrial and wearable Internet of things (IoTs). Recently, many works have convincingly demonstrated that PEH can also act as a self-powered sensor for detecting a wide range of machine and human contexts. These developments suggest that the same PEH hardware could be potentially used for simultaneous energy harvesting and sensing (SEHS), offering a new design space for low cost and low power IoT devices. Unfortunately, realization of SEHS is challenging as the energy harvesting process distorts the sensing signal. To achieve high quality sensing from PEH, the state-of-the-art uses separate PEHs for sensing and energy harvesting, which increases system complexity, form factor, and cost. In this paper, we propose a novel SEHS architecture, which combines energy harvesting and sensing in the same piece of PEH, and minimizes distortion in the sensing signal by applying a special filtering algorithm. We prototype the SEHS concept in the form factor of a shoe, and evaluate its energy harvesting as well as sensing performance with 20 subjects using gait recognition as a case study. We demonstrate that the SEHS prototype harvests up to 127% more energy and detects human gait with 8% higher accuracy while consuming 35% less power compared to the state-of-the-art.**

***Index Terms*—Piezoelectric Energy Harvesting, Simultaneous Energy Harvesting and Sensing, Context Detection from Energy Harvesting, Gait Recognition**

I. Introduction

Piezoelectric energy harvesting (PEH), which converts motion, stress, or vibration into usable electrical power, has become an attractive solution to power many industrial sensor nodes [1], [2]. The continuous improvement of PEH power density combined with rapid advancements in low-power electronics may soon bring PEH to wearable devices as well. As a matter of fact, devices that can harvest energy from human motion to charge a standby battery have already started to appear in the market [3]–[6].

An interesting recent development confirms that PEH can serve not only as a source of ambient power, but also as a sensor for detecting a wide range of machine and human contexts, such as measuring the air flow of heating and air conditioning systems [7], detecting the activities of daily living (ADL) [8], or even demodulating acoustic communications [9]. These findings suggest that the same PEH hardware could be potentially used for simultaneous energy harvesting and sensing (SEHS), offering a new design space for low cost and low power electronics for the rapidly growing Internet of Things of market. PEH-based sensing is expected to be more power-efficient than conventional sensor-based sensing because it does not require power supply for its operation. For example, a detailed power measurement study in [8] reveals that use of PEH for ADL detection could reduce 79% of the overall system power consumption of conventional accelerometer-based systems.

Unfortunately, realization of SEHS faces practical challenges arising from the interactions between the energy harvesting and sensing processes. In particular, when a capacitor is used to store the harvested energy from the PEH hardware, the dynamic states (stored energy) of the capacitor modifies the current or AC voltage signal generated by the PEH. Since context detection relies on the AC voltage signal of the PEH, its modification degrades the sensing or context detection performance of the PEH.

Most prior work on PEH-based sensing [10]–[12] only considered the sensing circuit without implementing energy harvesting and storage components, i.e., no capacitor was included in the circuit to store the harvested energy. The focus of these works was mainly to demonstrate that PEH is capable of sensing many contexts. As such, these works did not face the challenges involved in a true SEHS system. Although energy harvesting and storage were implemented in the PEH-based airflow sensing research [7], the authors used two separate PEH hardware in their system. One PEH was used for sensing only, and the other for energy harvesting and storage only. Indeed, the authors of [7] admitted that the sensing signal is damaged when the same PEH is used for both energy harvesting and sensing, hence they used separate PEH hardware to avoid the problem.

The focus of this paper is to devise solutions that enable use of the same PEH hardware for both energy harvesting and high quality sensing. In particular, we propose and demonstrate that high quality sensing for SEHS is achievable by using capacitor samples to filter out the impact of the capacitor on the AC sensing signal. On the one hand, the outcome directly reduces the cost and complexity of a SEHS system as separate PEH elements are no longer required for energy harvesting and sensing. On the other hand, when comparing with the state-of-the-art, total energy harvesting capacity can be increased if two PEHs are used, because both of them can harvest energy. On the same token, context detection accuracy can be increased when two PEHs are used, because both of them can act as

sensors providing multiple sensing signals.

The contributions of this paper can be summarized as follows:

- We propose a novel SEHS architecture to achieve simultaneous energy harvesting and sensing using the same PEH hardware. In this architecture, we minimize the harmful effect of energy harvesting on the sensing signal by applying a filtering algorithm to it.
- We design and implement a prototype of the proposed SEHS architecture using two PEHs inside a shoe, where each PEH simultaneously harvests energy as well as senses the gait of the user. To the best of our knowledge, this is the first implementation of SEHS reported in the open literature.
- We evaluate the performance of the SEHS prototype using 20 subjects. Our results demonstrate that the SEHS prototype can harvest up to 127% more energy and detect human gait with 8% higher accuracy compared to the state-of-the-art.
- We carry out a detailed power measurement to confirm that SEHS achieves the performance improvements while actually consuming less system power.

The rest of the paper is organized as follows. Section II presents the design of the proposed SEHS architecture including the filtering algorithm for minimizing the harmful effect of energy harvesting on information sensing. Prototyping of the SEHS architecture and its evaluation using gait recognition as a case study are described in Section III. Power measurements to quantify the overhead of the proposed filtering algorithm are presented in Section IV. We review the related works in Section V before concluding the paper in Section VI.

II. SEHS Design

In this section, we present the design of the proposed SEHS architecture, illustrate the effect of energy harvesting on the sensing signal, and explain the proposed filtering algorithm to minimize the effect of energy harvesting on information sensing. Let us first discuss the available design options for energy harvesting and sensing with PEH before presenting our own design.

A. Options for Energy Harvesting and Sensing with PEH

There are two potential architectures for energy harvesting and sensing with PEH as illustrated in Figure 1.

- **Separate PEHs (state-of-the-art):** In this architecture, one PEH hardware is used for energy harvesting and a separate PEH is used for sensing. Therefore, this option requires two PEHs to achieve both energy harvesting and sensing. The main benefit of this approach is that it completely avoids any interference between harvesting and sensing. This architecture is the state-of-the-art and adopted in [7], where the authors utilize one PEH to sense the speed of airflow and the other to harvest the energy generated from the vibrations caused by the airflow. In general, however, this architecture is inherently *inefficient* in the sense that it can harvest energy from only *one of the two deployed PEHs*. Similarly, only one of the two PEHs can be used for sensing, which wastes the opportunity to improve context detection performance by fusing sensing signals from both PEHs.
- **SEHS architecture (the proposed approach):** For a given PEH, this architecture performs energy harvesting and sensing at the same time. As such, it is subjected to the so-called *interference problem*, i.e., the energy harvesting may alter or distort the sensing signal, which may ultimately reduce the context detection accuracy. This approach, however, makes efficient use of PEH. For example, it enables both energy harvesting and sensing using a single PEH, which may be desirable for small form factor IoT devices. On the other hand, if two PEHs can be accommodated in the device, the proposed SEHS architecture can double the total amount of harvested energy compared to the state-of-the-art, which can harvest energy from only one of the two PEHs. Since every PEH is also capable of sensing, SEHS provides an opportunity to fuse sensing signals from two PEHs to potentially increase the accuracy of context detection. We will quantify the benefits of SEHS later in the paper using *gait recognition* as a case study.

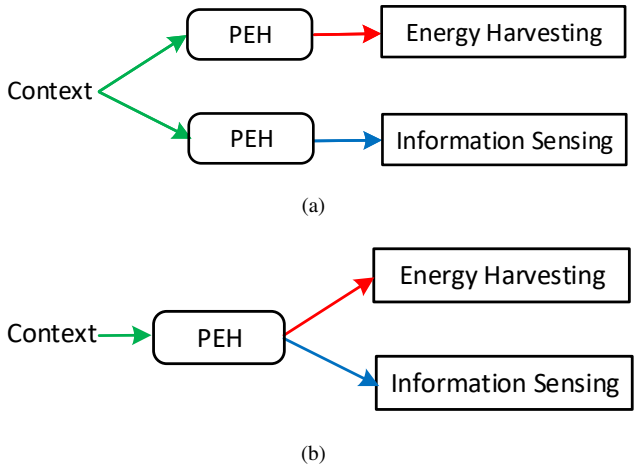

Fig. 1: Alternative architectures for energy harvesting and sensing with PEH: (a) State-of-the-art using separate PEHs for energy harvesting and sensing [7], and (b) the proposed SEHS architecture.

B. Design of the Proposed SEHS

The aims of the SEHS design are to (1) store the harvested energy, i.e., the rectified AC voltage generated by the PEH, in a capacitor, and (2) read the same AC voltage for context sensing using minimal power consumption. Unfortunately, reading the PEH AC voltage requires some additional processing, which would consume some power. Note that PEH generates electric potential proportional to the applied strain [13] and the polarization of the generated electricity corresponds to the direction of the induced deformation, producing alternating

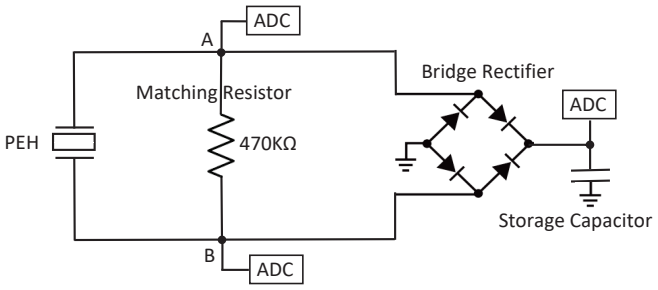

Fig. 2: Circuit design of the proposed SEHS architecture

voltage (AC). PEH usually generates an open-circuit AC voltage within *minus decades volts to decades volts* [14], while the commonly used ADC (Analog-to-Digital Converter) can only measure the non-negative voltage ranging from 0V to 5V. Consequently, the voltage signal cannot be acquired when PEH output is directly connected to ADC. To address this problem, most existing works utilize an *amplifier* [7], [15] or *voltage divide circuit* [11], [12] to measure the AC voltage using a single ADC channel, which consume *several hundreds of* μW.

One of our design goals is to minimize the sensing related power consumption. We achieve this by trading off *voltage divider* with additional ADC channels, as ADC channels consume very little power on the order of 1-2 microwatts (see Section IV for measurements). Figure 2 shows the circuit design of the proposed SEHS architecture. A matching resistor is used to limit the peak amplitude of the AC voltage within the ADC readable range. Instead of using a single ADC channel to capture the whole AC waveform, we use two ADC channels, i.e., point A (V_A) and point B (V_B), to measure the voltage on the matching resistor. Since the two points are directly connected to the output of PEH, the generated voltage, V, can be easily derived by subtracting the measured voltage at point B from point A (both are non-negative values), i.e., $V = V_A - V_B$. The energy flows to the capacitor through a full-bridge rectifier which is used to convert the AC voltage to DC voltage. With this circuit, the proposed SEHS architecture is able to collect the voltage signal and store the generated energy by using the same piece of PEH hardware.

C. Effect of Energy Harvesting on Sensing

Unfortunately, when a capacitor is used to store the harvested energy, its dynamic states (stored energy) modifies the current or AC voltage signal generated by the PEH. To illustrate the effect of energy harvesting on AC voltage reading, we collected some data when our circuit was used in the shoe of a waking subject (see Section III-A for prototype details). Figure 3 illustrates the waveform of the sampled AC voltage signal as well as the capacitor voltage. Intuitively, the peak-to-peak amplitude of the AC voltage should be approximately identical, as the entire trace is extracted from the same person while walking with a consistent style [16]. However, we can see that the peak-to-peak amplitude of the

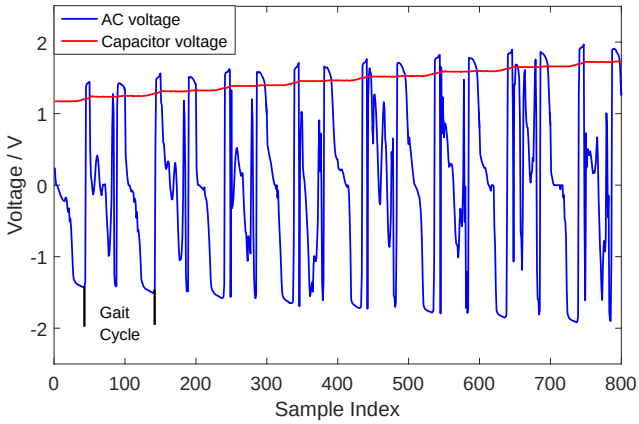

Fig. 3: The original AC voltage and capacitor voltage

AC voltage is actually increasing with time as the capacitor voltage rises, i.e., more energy is being stored. The similar phenomenon is also described in [7].

The observed effect of energy harvesting on AC voltage in Figure 3 can be explained as follows. Using capacitor theory [17], Figure 4 illustrates how the charging current decreases while the capacitor is being charged. This theory suggests that the current flow to the PEH is dropping when energy is being harvested and stored in the capacitor. Note that the PEH has a large internal resistance on the order of MΩ [7], [18] and the output voltage is determined by the load resistance as well as the internal resistance [18], [19]. With the current flow decreased, the voltage on the internal resistance of PEH is reduced. As a result, the amplitude of the output voltage is increased, which explains the increasing peak-to-peak amplitude of the AC voltage in Figure 3.

How to minimize the distortion of the sensing signal in a SEHS architecture remains an open problem. Note that the state-of-the-art in [7] did not actually solve this problem, but instead used two separate PEHs to avoid this issue. In the following subsection, we propose a filtering algorithm that can minimize the distortion effect of energy harvesting on the sensing signal.

D. Filtering Algorithm

Algorithm 1 shows the proposed filtering algorithm to minimize the effect of capacitor charging on the AC voltage readings. Note that the main effect is on the AC voltage amplitude, where the amplitude continues to increase with increasing capacitor voltage. The aim of the filtering algorithm, therefore, is to prevent the increasing capacitor voltage from lifting the AC voltage *without destroying the pattern of the signal*. This is achieved by introducing a constant, V^*, in lines 4 and 6 in Algorithm 1. The output, $V^{'}(t)$, is the *filtered* sensing signal.

The algorithm will work correctly, i.e., the filtered signal will have the same pattern as the original signal, for any positive values of V^*. However, the larger the V^*, the higher the amplitude of the filtered signal, and vice versa. Figure 5

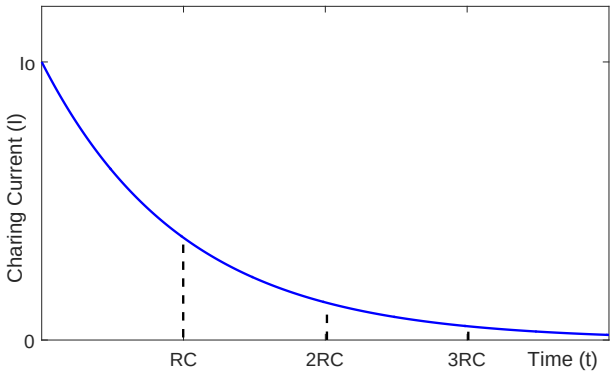

Fig. 4: Charging current as a function of time. RC is the time constant and I_0 is the initial current when capacitor voltage is 0.

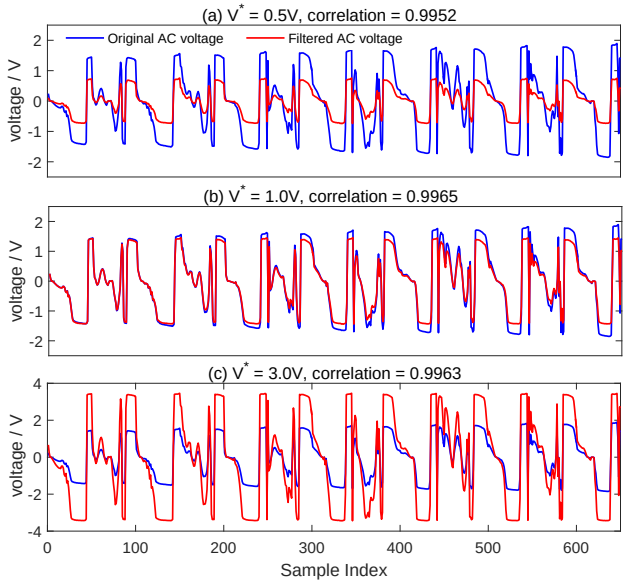

Fig. 5: Comparison of AC voltage with and without filtering.

compares the waveform of the original AC voltage (blue) and the filtered version (red) for different values of V^*. We can see that irrespective of the value chosen for V^*, the filtered signal matches well with the original signal, which can be verified easily from visual inspection, as well as from the high correlation values. Although, as predicted, the amplitude of the filtered signal is affected by the choice of V^*, we will demonstrate that the sensing performance is not influenced in Section III-E1.

The complexity of the filter is $O(N)$ (N is the number of samples), which suggests that it can be implemented without significant computational burden. Note that the filter requires the capacitor voltage (V_C) as input, which can be easily obtained using an additional ADC channel as shown in our circuit design (Figure 2). Use of additional ADC channels contribute minimal power consumption overhead as will be demonstrated in our measurements in Section IV.

Algorithm 1: Proposed Filtering Algorithm

Input: $V_A(t), V_B(t), V_C(t), V^*$
Output: $V_A^{'}(t)$, $V_B^{'}(t)$, $V^{'}(t)$

Main procedure:
for *t = 1, 2, ..., N* **do**
  if $V_A(t) \geq V_C(t$ **then**
    $V_A^{'}(t) = V_A(t) - V_C(t) + V^*$;
  else
    $V_A^{'}(t) = V^* * (V_A(t)/V_C(t))$;
  end
  the same operation for $V_B(t)$;
  obtain $V_B^{'}(t)$;
  $V^{'}(t)$ **=** $V_A^{'}(t)$ **-** $V_B^{'}(t)$;
end

III. Gait Recognition with SEHS

In this section, we evaluate the performance of the proposed SEHS architecture using gait recognition as a case study.

A. SEHS Prototyping

Figure 6 shows the prototype we designed and implemented in the form factor of a shoe to harvest energy during human walking and detect the user gait at the same time using the PEH voltage signal. To explore the potential performance improvements compared to the state-of-the-art, the prototype includes two PEHs from Piezo System [20] mounted on the front and rear of the insole. AC voltages from the PEHs are rectified by full-bridge diodes rectifier and charged into two $1000\mu F$ electrolytic capacitors. The output voltage and capacitor voltage are sampled by an Arduino 101 [21] board, which is equipped with an Intel Curie microcontroller. A sampling rate of 100Hz is used for data collection and the sampled data is saved on a 4GB microSD connected to the Arduino using a microSD shield. A nine volts battery powers the whole system. To help users collect data, the prototype contains three switches, one is to control the start and stop of data collection and the other two for controlling the charging and discharging of the two capacitors respectively. The entire Arduino board is placed outside the shoe.

The Arduino 101 measures voltage between 0 and 5 volts and provides 10 bits of resolution, i.e., 1024 different values. The corresponding output voltages from the measurements, therefore, are obtained as:

$$voltage = \frac{5 * ADCmeasurement}{1024} \quad (1)$$

By measuring the capacitor voltage, we can calculate the amount of the stored energy using the following equation:

$$E = \frac{1}{2}CV^2 \quad (2)$$

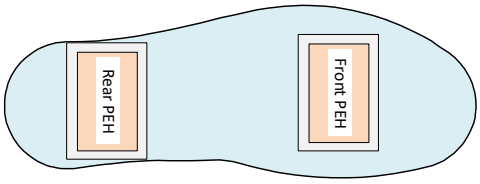

(a) Placement of PEHs on the insole

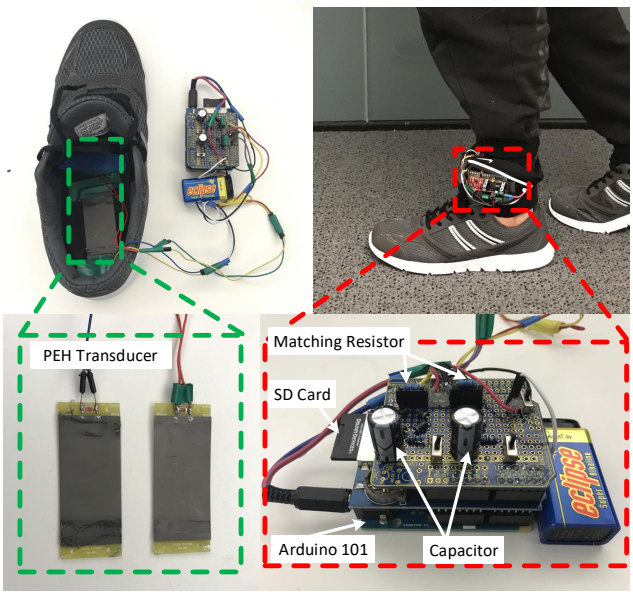

(b) Circuit design and placement during walking

Fig. 6: The design and appearance of the SEHS prototype.

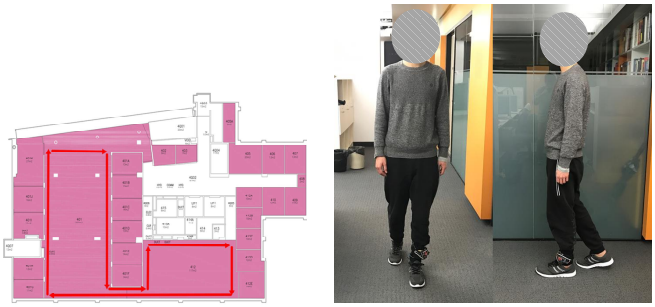

(a) Experiment environment (b) Subject Walking

Fig. 7: Data collection setup

B. Data Collection

During the data acquisition stage, we create the dataset by asking 20 healthy volunteers, including 16 males and 4 females[1], to walk along the specified route as shown in Figure 7(a). Each volunteer is asked to wear a shoe equipped with the designed insole in their left foot and the data collection module is attached to the ankle position as shown in Figure 7(b). The participants are suggested to walk in his/her normal walking style and speed. The data collection duration is approximately 300 seconds and the subjects need to toggle the switch to discharge the capacitors every 50 seconds. The reason is that the accumulated voltage on the capacitor will exceed $5V$ when walking for a certain period of time(around 55 seconds in our tests), so that it can not be measured. More importantly, the high voltage may damage the ADC module of the board.

C. Gait Recognition Methodology

Figure 8 illustrates the overall system model of gait recognition using SEHS. An insole is equipped two PEHs to harvest the energy as well as detect the gait of the wearer. The generated AC voltage is rectified and the collected energy flows to the capacitor. A filter, which uses the capacitor voltage as an input, is used to minimize the interference of the energy storage on the AC voltage signal. Thus, we have five different options for gait recognition, the original signal from the front PEH (option 1), the filtered signal from the front PEH (option 2), the original signal from the rear PEH (option 3), the filtered signal from the rear PEH (option 4), and finally the fused signal, which combines signals from both front and rear (option 5). We will compute and compare gait recognition accuracies for all these options.

We collect a time series of voltage signal of the PEHs when subjects are walking, in which the signal follows a cyclic pattern reflecting the gait of each subject. As shown in Figure 3, there are two peaks within one gait cycle, which indicate the heel strike and toe-off time of the foot respectively. Firstly, the moving average function and a low pass filter with the cutoff frequency of 10Hz are employed to eliminate out-band interference. We then apply a band pass filter to detect these peaks and the gait cycle is obtained by combining the samples between two consecutive peaks together. Since the walking pattern varies from different subjects, we tune the lower and upper cutoff frequency of the band pass filter for each subject ranging from 0.5Hz to 3Hz to enable an accurate gait cycle segmentation.

After the peak detection and samples combination, gait cycles with different time duration are available. Figure 9 plots the distribution of the gait cycle duration of the 20 subjects who are suggested to walk in their normal speed. It is clear that the time duration of one gait cycle varies from 0.8s to 1.3s. To deal with such variable walking speeds which may occur among different subjects or one subject in different walking scenarios, we perform the linear interpolation on the detected gait cycles. According to the distribution of the gait cycle length, the number of samples in one gait cycle ranges from 80 to 130 with the sampling rate of 100Hz. Thus, we interpolate the gait cycles to equal length with 130 samples.

Accurate gait pattern extraction is the critical factor that affects the gait recognition accuracy. In our experiment, volunteers were asked to walk in a square environment as shown in

[1]Ethical approval for carrying out this experiment has been granted by the corresponding organization (Approval Number HC15888).

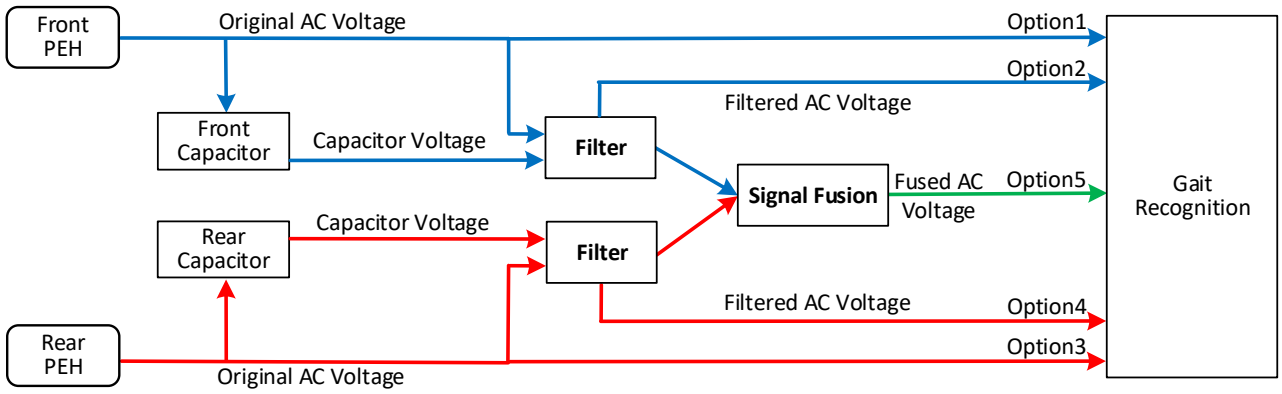

Fig. 8: System model of gait recognition using SEHS.

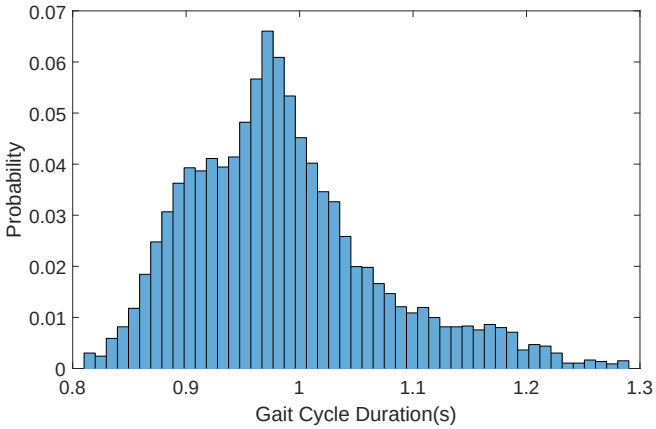

Fig. 9: The distribution of gait cycle duration

Figure 7(a) for several minutes, during which they experienced decades of turnings and some short pauses. Obviously, the detected gait cycles within these periods contain distorted gait pattern. Therefore, it is requisite to omit these unusual cycles to keep a high recognition accuracy.

We perform Dynamic Time Warping (DTW) function to delete *unusual cycles* for each subject. In detail, the average distance of all the gait cycles are computed firstly and treated as the typical cycle. Then, the distance between each cycle and the typical cycle is calculated. We detect and omit the irregular cycles by a simple threshold method, i.e. if the DTW distance of a detected cycle is higher than a predefined value, it will be dropped. The DTW distance reflects the similarity among a given cycle and the rest cycles of the subject. We collect around 280 to 300 gait cycles for each subject. To achieve a fair classification, we extract 250 gait cycles per subject after performing irregular cycle deletion. In total, a 2x20x250 gait cycle dataset is created and utilized to evaluate the performance of the proposed SEHS architecture and filter.

Motivated by the multi-sensor mechanism [22], we also explore signal fusion methods to enhance the sensing performance. Here, we investigate two signal fusion approaches, i.e., concatenation and intersection. Assuming that we have got two signals X, Y with the size of N. Without fusion, the two signals can be used as information for a given sensing application alone. When considering signal concatenation, we fuse the two signals in the following way:

$$XY_{\_Con} = [X_1, X_2, ..., X_N, Y_1, Y_2, ..., Y_N] \tag{3}$$

While for signal intersection, the two gait cycles are combined as:

$$XY_{\_Int} = [X_1, Y_1, X_2, Y_2, ..., X_N, Y_N] \tag{4}$$

We explore whether signal fusion can achieve better sensing performance in Section III-E4.

To this end, the extracted gait cycles are ready for classification. In this paper, we consider three classifiers: Support Vector Machine (SVM) and K-Nearest Neighbor (KNN), and Sparse Representation based Classification (SRC) [23], [24]. SVM and KNN are two traditional classifiers with a wide range of sensing applications like human activity recognition [11], while SRC is an emerging classifier that has been proved to be more robust to environmental noise in sensing tasks [16], [25]. The gait recognition accuracy of using different classifiers will be compared in Section III-E3.

During classification, each gait cycle is regarded as a sample or vector for training or testing. As SRC can be used as a feature-less classifier, we use the time domain signals, i.e. gait cycle vectors, for model training and testing. For SVM and KNN, we first extract features for every gait cycle signal and then deliver these features as the input to the classifier. Referring to [11], we extract 22 features from both time domain and frequency domain, such as *Mean, Skewness, Q1, Dominant frequency* and many more, which have already been demonstrated effective in recognition tasks.

D. Performance Metrics

In this section, we evaluate the performance of the proposed SEHS architecture and filter based on the collected dataset in the following five aspects. Firstly, we use the DTW distance to explore the effectiveness of the proposed filtering

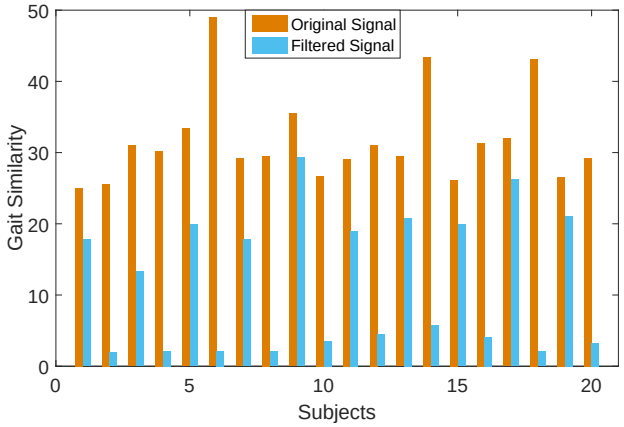

Fig. 10: Gait similarities for the original vs. the filtered signals.

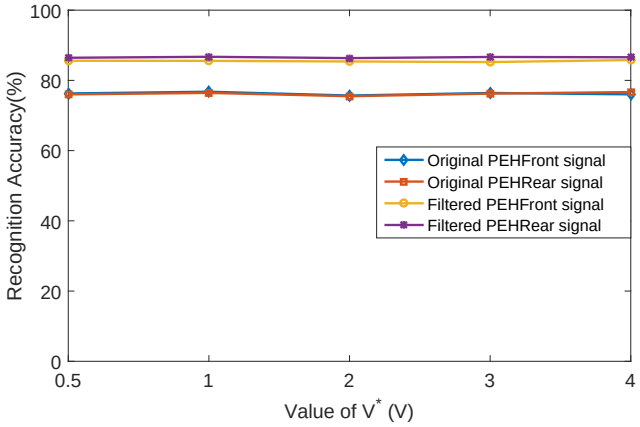

Fig. 11: Recognition accuracy v.s. Value of V^*

algorithm from the signal waveform aspect. Secondly, the gait recognition accuracy with different system parameters, such as sampling rate and classifier, is derived to evaluate the performance of the filter and signal fusion. Thirdly, as gait information has been widely studied for authentication in the literatures [16], [26], [27], we also explore the performance of the filter on the gait authentication system in terms of the equal error rate. Afterwards, the comparison of the proposed SEHS architecture with the separated PEH architecture is investigated from both energy harvesting and sensing aspects. Finally, as the filter requires capacitor voltage as input, we explore its practicability by measuring the power overhead of sampling the capacitor voltage.

We summarize the evaluation metrics used in this paper as follows:

- **Recognition accuracy**: represents the percentage of correctly classified test samples, which is the main parameter to assess the recognition system.
- **False positive rate (FPR)**: indicates the probability that an imposter is wrongly recognized as a legitimate user, which reflects the security level of the authentication system.
- **False negative rate (FNR)**: indicates the probability that a legitimate user is falsely rejected, which reflects the user experience of the legitimate user.
- **Equal error rate (EER)**: the EER is the location on a DET (Decision Error Trade-off) curve where the FNR and FPR are equal, which indicates the *overall* performance of the authentication system.
- **Amount of Energy per Step**: to evaluate the performance of energy harvesting, we computed the amount of energy generated each step using the capacitor voltage.

E. Results

1) Filter Performance: Since gait cycles of the same person are expected to be similar during a normal walk, such *gait similarity* can be used to assess the performance of the proposed filter algorithm. As energy harvesting distorts the AC sensing signals for gaits, we can expect that the gait similarity for the original AC signal would be low, but would increase when the filter is applied. For each subject and each PEH, we computed gait similarity for a given trace of 250 gait cycles as the average DTW (dynamic time warping) between all possible pairs of gait cycles. For the original and the filtered signals, Figure 10 compares gait similarity averaged over the two PEHs for each of the 20 subjects. The gait similarity is reflected by the DTW distance in the figure, where the lower the Y-axis value, the higher the gait similarity. We can clearly see that the gait similarities for the filtered signal are consistently higher than those for the original signal. This provides evidence that the proposed filtering algorithm has successfully reduced signal distortions caused by energy harvesting.

As mentioned in Section II-D, the value of V^* used in our filtering algorithm does not affect the correlation between the original signal and the filtered signal, although the amplitude of the filtered signal diverse We further explore the gait recognition accuracy when choosing different values of V^*. As shown in Figure 11, all the four signals with and without filtering produce almost the same gait recognition accuracy with the value of V^* ranging from 0.5V to 4V. This proves that the performance of the filtering algorithm is irrespective of V^*.

2) Gait Recognition Accuracy vs. Sampling Rates: For different sampling rates, Figure 12 compares *gait recognition accuracies*, i.e., the percentage of correctly classified test samples, obtained with and without filtering for both PEHs (*PEHFront* and *PEHRear* refer to the front and rear PEH respectively) using the SRC classifier. It is clear that for all sampling rates, filtering significantly improves the gait recognition accuracy. For both signals, a minimum of 40 Hz is required to achieve high recognition accuracy. In the subsequent analyses, we will therefore consider a sampling rate of 40 Hz.

It is interesting to note that gait recognition accuracies of the *PEHFront* and *PEHRear* signals are almost identical, which indicates that both the signals contain significant gait

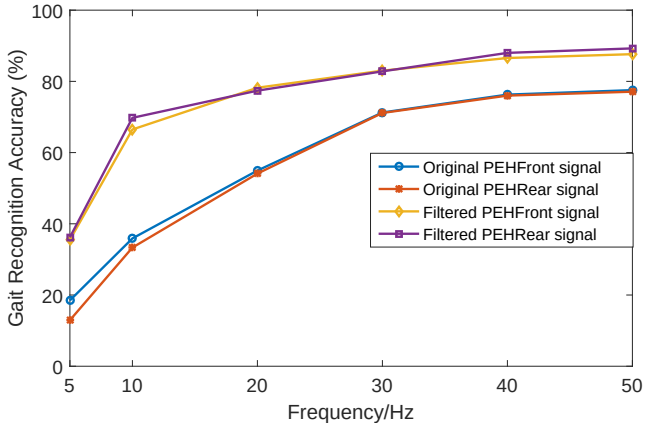

Fig. 12: Recognition accuracy v.s. Sampling rate

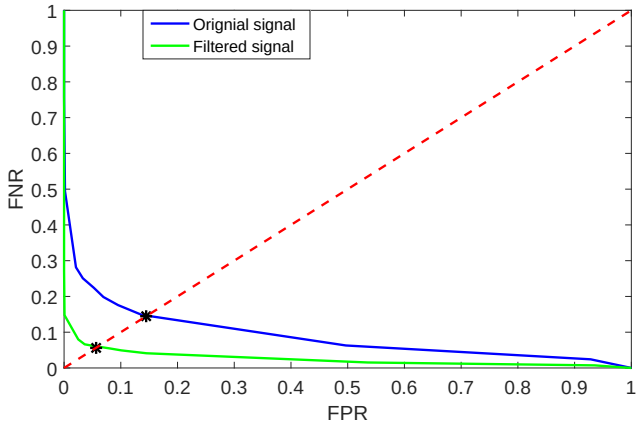

Fig. 13: DET curve in authentication system

TABLE I: Recognition accuracy v.s. classifiers

Classifier	Original signals		Filtered signals	
	PEHFront	PEHRear	PEHFront	PEHRear
KNN	54.3%	50.7%	62.9%	60.3%
SVM	66.7%	65.8%	74.4%	72.8%
SRC	76.28%	76.01%	85.56%	86.72%

TABLE II: Recognition accuracy with signal fusion

PEHFront	PEHRear	Intersection	Concatenation
85.56%	86.72%	95.07%	95.85%

information. As a result, it may be possible to increase the gait recognition accuracy by fusing the signal from the front with the one from the rear. Indeed, such fusion opportunities are explored later in the section. Note that with the state-of-the-art architecture, which uses one PEH for sensing and one for energy harvesting, such fusion opportunities do not exist.

3) Gait Recognition Accuracy vs. Classifiers: In this section, we evaluate the gait recognition performance of the filter for different classifiers. The parameters in SVM and KNN are tuned to provide the highest accuracy. For SVM classifier, we choose *quadratic kernel* and the *box constraint level* is set to 5. For KNN classifier, the number of nearest neighbors is set to 10. For each classifier, we perform 10-fold cross-validation on the collected dataset and present the average recognition accuracy.

Table I presents the gait recognition accuracy of the three classification methods. We can clearly see that the filtered signals outperform the original counterparts for all the three classifiers. An accuracy improvement of 8% - 10% is achieved when the filter is applied, which provides strong evidence that the proposed filter is robust and effective across the choice of classifiers. Our results also validate previous findings [28]–[30] that SRC has superior context recognition capabilities than many other classifiers. However, even the SRC struggles to achieve a high gait recognition accuracy when the signal is distorted by energy harvesting, it can be improved to 86% by applying the proposed filter.

4) Improving Gait Recognition with Signal Fusion: As mentioned earlier, the proposed SEHS architecture offers signal fusion opportunity when two PEHs are used. In this section, we quantify the benefits of such signal fusion in improving the gait recognition accuracy. As explained in Section III-C, we consider two signal fusion approaches: *concatenation* and *intersection*. Table II compares the gait recognition accuracy of using the signals obtained via the two methods for SRC and 40 Hz sampling rate. It can be seen that both fusion methods improve gait recognition accuracy by about 10%. The reason is that the combined signal takes advantage of the gait information from different positions in the foot to build a more accurate gait model for each subject.

5) Improvement of Gait Authentication Performance: In this section, we investigate the system performance when using PEH signal to perform gait authentication. We consider the scenario of passive attackers, which may be occurred when the insole is worn by other people who attempt to access the system. We conduct this experiment by dividing the 20 subjects into two groups (10 subjects in each group), in which one group is set as imposters and the rest are genuine users. Here the training and testing datasets are obtained from the concatenated signal and SRC is chosen as the classifier. We then reverse the roles and repeat the experiment.

The comparison of original signal and filtered signal is presented with the Decision Error Trade-off (DET) curve as shown in Figure 13. The DET curve is obtained by setting different confidence levels and then calculating the corresponding FPRs and FNRs. The red dash line stands for the potential points of EER. In the figure, the crossovers of the red dash line and the FPR - FNR curve are the locations of EER. It can be seen that the EER when using the original signal and filtered signal is 14.5% and 5.7% respectively, which means that out of 100 genuine users 6 are falsely rejected and out of 100 attackers 6 are wrongly accepted in the best case.

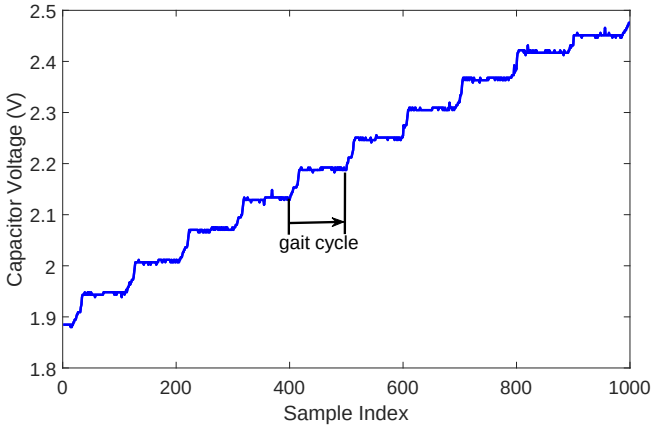

Fig. 14: Capacitor voltage

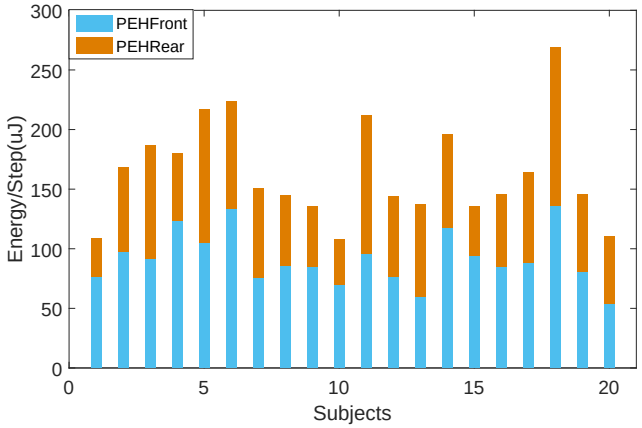

Fig. 15: The amount of energy generated per step from the two PEHs. The average generated energy of *PEHFront*, *PEHRear* and total is around $92uJ$, $72uJ$ and $164uJ$ respectively

An improvement of 9% is achieved with the filtering. The results reveal that the proposed filter not only improves the gait recognition accuracy but also promote the system security as well as the user experience in the gait authentication system.

The filtering algorithm is designed to minimize the amplitude interference on the original signal, and its performance on gait recognition has been demonstrated. Moreover, we can expect that the performance is also potential for other sensing applications, such as activity recognition, as *Mean Amplitude* and *Maximum Amplitude* are high importance features for classifying different activities as indicated in [11] (Table V).

6) Analysis of Harvested Energy: In SEHS, not only the voltage signal is collected, but also the generated energy by human waling is stored in the two capacitors. By measuring the capacitor voltage, we can calculate the amount of generated energy from different PEHs and subjects using Equation 2.

Figure 14 presents the capacitor voltage of one subject, in which each *stair* corresponds to one gait cycle. The *stair* suggests that the energy is only produced within a small time slot, where the capacitor voltage climbs sharply, during each gait cycle. The distribution of the average generated energy per step of the 20 subjects from the two PEHs is shown in Figure 15. It is apparent that the total amount of the harvested energy varies with different people ranging from $109uJ/step$ to $269uJ/step$ with an average of $164uJ/step$. Assume that people walk in 2Hz, i.e., one gait cycle each second, a power output of $164uW$ is achieved by wearing the insole in one foot, which is encouraging to extend the battery lifetime or even replace the battery for wearable devices.

Compared to the separated PEH architecture where only one PEH is capable to harvest energy, the proposed SEHS architecture increases the amount of average generated energy.In detail, when using the front PEH for energy harvesting, 78% more energy is harvested in SHES, whereas up to 127% more energy is harvested when the rear PEH is considered as the energy harvester. From the sensing aspect, as the SEHS enables two PEHs as the sensors for detecting the gait information, the recognition accuracy is also promoted with signal fusion as discussed in Section III-E4.

IV. Power Consumption Measurements

In the previous sections, we have demonstrated the superior performance of the proposed SEHS architecture in terms of both energy harvesting and context detection. However, the *filter* in our prototype requires the capacitor voltage samples as an input, which is not used in the state-of-the-art. Consequently, the power consumption overhead of sampling the capacitor voltage should be measured to assess the practicability of the filter. In fact, for each PEH, the proposed SEHS architecture uses a total of three ADCs, which means a total of six ADCs are used for a dual-PEH SEHS. Sensing power consumption of SEHS therefore can be measured by simply measuring the power consumption of sampling the ADCs. In this section, we carry out these measurements first and then use the measured power consumption data to compare the sensing power consumption for SEHS against that of the state-of-the-art.

A. Measurement setup

We select the Texas Instrument SensorTag as the target device, which is equipped with an ultra-low power ARM Cortex-M3 MCU and 12-bits ADC. The SensorTag is running with the Contiki 3.0 operating system. Figure 16 shows the experiment setup, where a Tektronix TBS-1052B digital oscilloscope is used to measure the current draw of the SensorTag. A 10Ω resistor is connected in series between the SensorTag and a 3V coin battery. We connect the probes of the oscilloscope across the resistor, so that the current draw can be calculated using the captured voltage and the resistance. We load three programs for sampling one, three, and six ADC channels, respectively.

B. Power consumption analysis

Figure 17 illustrates the profiling of an ADC sampling event. At the beginning, the MCU is in *deep sleep* mode. Once the ADC sampling event is triggered, MCU wakes up and reads

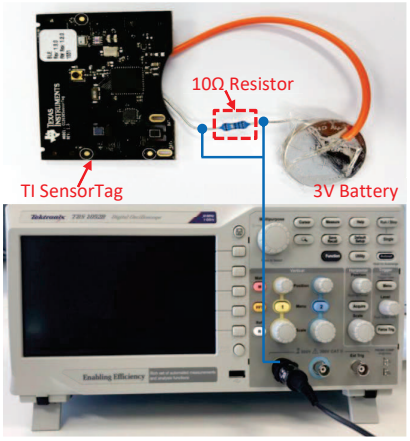

Fig. 16: Measurement setup

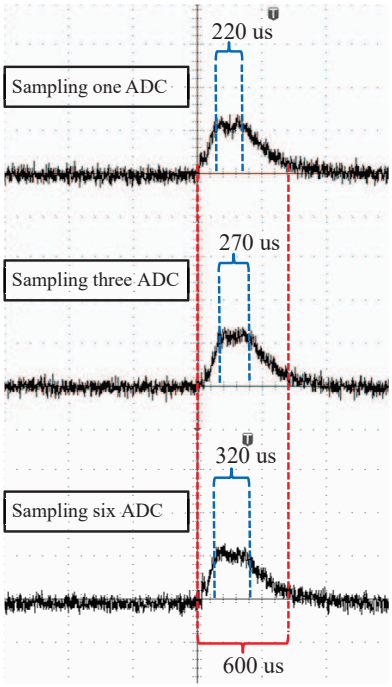

Fig. 17: Profiling of ADC sampling (need to be replaced)

the value from ADC channels and then goes back to deep sleep mode. We can observe that the total time of the three events are almost equal (marked with red dashed line), while the major difference comes from the time duration that the MCU is turned on (marked with blue dashed line). Note that the process of MCU turning on/off requires time, which refers to the *climbing* and *dropping* stage in the profiling. As shown in the figure, the MCU is turned on for $220\mu s$, $270\mu s$, and $320\mu s$ when sampling one, three, and six ADC channels, respectively.

Table III presents the average power consumption data for sampling at a rate of 40 Hz. The *MCU On* time denotes the period when MCU is sampling ADC after turned on and the *total event* time denotes the duration of the sampling event including the preparation of the MCU. The data in the Power column, which denotes the average power consumption for the entire duration of the event, is directly obtained by using the built-in function of the oscilloscope. We then calculate the energy consumed during one single sampling event in the following column. The last column shows the average power consumption when duty-cycling is performed at a sampling rate of 40Hz (note that the power consumption of MCU in deep sleep mode was $6\mu W$ according to our measurement). The first row of the last column represents power consumption of the state-of-the-art architecture [7], which uses an amplifier (which consumes $500\mu W$) with one ADC channel.

It can be seen that the average power consumption of the state-of-the-art, where both MCU and amplifier are considered, is $29.43\mu W$. A single-PEH SEHS requires three ADC channels and consumes an average power of $18.12\mu W$, which reduces sensing power consumption by 38%. Even if we use a dual-PEH SEHS for improved energy harvesting and context detection performance, we can still reduce the average power consumption by 35%. These results suggest that the proposed SEHS not only achieves better system performance in terms of energy harvesting and sensing, but also decreases the sensing power consumption compared to the state-of-the-art.

V. Related Work

In general, most existing works on piezoelectric energy harvesting can be classified into two categories: energy harvesting and context sensing. The basic principle is that piezoelectric material can produce AC voltage when subjected to mechanical stress due to the piezoelectric effect.

In terms of energy harvesting, vibration based [31]–[33] and stress based [18], [34]–[36] mechanisms arouse many research interests. In particular, Tolentino et al. designed a self-sustained vehicular tracking system by absorbing energy from vehicle motor vibrations via the PEH [31]. Huang et al. [18] proposed a shoe based battery-free wearable sensing platform where the power comes from the two feet when people are walking. The designed PEH achieves a power output of 1-$2mW$, which enables the operation of sensors, MCU and radio with reasonable duty-cycling.

On the other hand, a variety of sensing applications are enabled by PEH signal as the output AC voltage of the PEH contains the signature of the context. In [10], a necklace equipped with the PEH is designed to capture the throat motions during eating. Using the AC voltage signal, different types of food, such as water, sandwich and chips, can be detected with good accuracy, thereby estimating the eating habits of the user. In [9], the authors leverage the PEH as a receiver for acoustic communication. The underlying idea is that the PEH is able to capture the air vibrations caused by the acoustic wave. By using the pattern of the generated AC voltage, the transmitted information can be demodulated through the proposed OOK method.

Interestingly, instead of using the AC voltage signal, recent works [37], [38] explored the feasibility of using the

TABLE III: Average power consumption of sampling at 40 Hz

Event	Time(us)		Power(uW)	Energy/Event(uJ)	Average power(uW)
	MCU On	total event			
One ADC	220	600	482	0.29	29.43
Three ADC	270	600	511	0.31	18.12
Six ADC	320	600	553	0.33	19.13

accumulated power signals, i.e. capacitor voltage, for sensing. In [37], the energy generated by human daily activities are stored in the capacitor. By using the capacitor voltage, five common activities are recognized with good accuracy, while the power consumption in sampling is reduced by 99% as merely 0.2Hz sampling rate is required. Similarly, the authors in [38] developed an energy-harvesting power meter architecture by utilizing the electromagnetic energy harvester. The harvested energy from the power line is stored in a capacitor to power and trigger the signal transmission of a wireless sensor node once the capacitor voltage reaches a predefined threshold. Using the signal receiving frequency, the power consumption can be estimated.

Using the PEH for either energy harvesting or sensing has been well investigated in the literature, but to achieve simultaneous energy harvesting and sensing is not trivial. Although the authors in [39] conceived the idea of simultaneous energy harvesting and sensing for unmanned aerial vehicle (UAV) stability control, the combined performance of harvesting and sensing was evaluated theoretically only. Their practical experiments confined to energy harvesting and gust alleviation separately. In [7], the authors implemented the two functions in the airflow sensing system, while two PEHs (one for energy harvesting and the other for sensing) are exploited for separate tasks, which increases the system complexity, form factor, and lowers the utilization efficiency of PEH.

The concept of SEHS is quite similar to SWIPT (simultaneous wireless information and power transfer) in wireless energy harvesting networks, where the RF signals are used for delivering energy as well as for transporting information [40]–[42]. To achieve SWIPT, the receiver architecture requires modification as the power sensitivity for energy harvesting and information reception is different. Thus, a variety of designs, such as antenna-switching [41], time-switching [43], power-splitting [44] and integrated architecture [45], are developed to optimize the system performance.

VI. Conclusion

We have proposed SEHS, a novel architecture for simultaneous energy harvesting and sensing using the same piece of PEH hardware. Compared to the state-of-the-art, which uses two separate PEHs each dedicated to *either energy harvesting or sensing*, the proposed SEHS architecture has several benefits. For example, SEHS can also use two PEHs, but each hardware can be exploited for *both energy harvesting and sensing*. Thus, SEHS can harvest twice as much energy with potential for increased sensing accuracy due to generating two distinct sensing signals from two PEHs. Taking gait recognition as a case study, we developed an insole-based prototype of SEHS to harvest energy as well as detecting the user gait. Based on the experimental data from 20 subjects, we have demonstrated that the SEHS prototype can harvest up to 127% more energy and detect human gait with 10% higher accuracy compared to the state-of-the-art. A detailed power measurement confirms that SEHS achieves these performance improvements while actually consuming less power.

References

[1] S. Sudevalayam and P. Kulkarni, "Energy harvesting sensor nodes: Survey and implications," *IEEE Communications Surveys & Tutorials*, vol. 13, no. 3, pp. 443–461, 2011.

[2] R. J. Vullers, R. Van Schaijk, H. J. Visser, J. Penders, and C. Van Hoof, "Energy harvesting for autonomous wireless sensor networks," *IEEE Solid-State Circuits Magazine*, vol. 2, no. 2, pp. 29–38, 2010.

[3] "AMPY," http://www.getampy.com/ampy-move.html//.

[4] "SOLEPOWER," http://www.solepowertech.com/.

[5] "KINERGIZER," http://kinergizer.com/.

[6] "Kinetic," http://www.seiko-cleanenergy.com/watches/kinetic-1.html.

[7] T. Xiang, Z. Chi, F. Li, J. Luo, L. Tang, L. Zhao, and Y. Yang, "Powering indoor sensing with airflows: a trinity of energy harvesting, synchronous duty-cycling, and sensing," in *Proceedings of the 11th ACM Conference on Embedded Networked Sensor Systems*. ACM, 2013, p. 16.

[8] S. Khalifa, G. Lan, M. Hassan, A. Seneviratne, and S. K. Das, "Harke: Human activity recognition from kinetic energy harvesting data in wearable devices," *IEEE Transactions on Mobile Computing*, 2017.

[9] G. Lan, W. Xu, S. Khalifa, M. Hassan, and W. Hu, "Veh-com: Demodulating vibration energy harvesting for short range communication," in *Pervasive Computing and Communications (PerCom), 2017 IEEE International Conference on*. IEEE, 2017, pp. 170–179.

[10] H. Kalantarian, N. Alshurafa, T. Le, and M. Sarrafzadeh, "Monitoring eating habits using a piezoelectric sensor-based necklace," *Computers in biology and medicine*, vol. 58, pp. 46–55, 2015.

[11] S. Khalifa, M. Hassan, and A. Seneviratne, "Pervasive self-powered human activity recognition without the accelerometer," in *Pervasive Computing and Communications (PerCom), 2015 IEEE International Conference on*. IEEE, 2015, pp. 79–86.

[12] G. Lan, W. Xu, S. Khalifa, M. Hassan, and W. Hu, "Transportation mode detection using kinetic energy harvesting wearables," in *Pervasive Computing and Communication Workshops (PerCom Workshops), 2016 IEEE International Conference on*. IEEE, 2016, pp. 1–4.

[13] G. Poulin, E. Sarraute, and F. Costa, "Generation of electrical energy for portable devices: Comparative study of an electromagnetic and a piezoelectric system," *Sensors and Actuators A: physical*, vol. 116, no. 3, pp. 461–471, 2004.

[14] C. Bowen, H. Kim, P. Weaver, and S. Dunn, "Piezoelectric and ferroelectric materials and structures for energy harvesting applications," *Energy & Environmental Science*, vol. 7, no. 1, pp. 25–44, 2014.

[15] Q. Lin, Y. Cui, S. Jiang, T. Ma, W. Xu, and W. Hu, "Poster: Automatic key generation using motion energy harvesters," *Proceedings of NDSS*, 2016.

[16] W. Xu, G. Lan, Q. Lin, S. Khalifa, N. Bergmann, M. Hassan, and H. Wen, "Keh-gait: Towards a mobile healthcare user authentication system by kinetic energy harvesting," in *Proceedings of NDSS*, 2017.

[17] H. Zhong, Z. Xu, X. Zou, Y. Zou, L. Yang, and Z. Chao, "Current characteristic of high voltage capacitor charging power supply using a series resonant topology," in *Industrial Electronics Society, 2003. IECON'03. The 29th Annual Conference of the IEEE*, vol. 1. IEEE, 2003, pp. 373–377.

[18] Q. Huang, Y. Mei, W. Wang, and Q. Zhang, "Battery-free sensing platform for wearable devices: The synergy between two feet," in *Computer Communications, IEEE INFOCOM 2016-The 35th Annual IEEE International Conference on*. IEEE, 2016, pp. 1–9.

[19] H. A. Sodano, G. Park, and D. Inman, "Estimation of electric charge output for piezoelectric energy harvesting," *Strain*, vol. 40, no. 2, pp. 49–58, 2004.

[20] "Piezo system," http://www.piezo.com/.

[21] "Arduino 101," https://www.arduino.cc/, accessed: 2017-10-04.

[22] D. L. Hall and J. Llinas, "Multisensor data fusion," *Handbook Multisensor Data Fusion: Theory and Practice,*, 2017.

[23] K. Huang and S. Aviyente, "Sparse representation for signal classification," in *Advances in neural information processing systems*, 2007, pp. 609–616.

[24] J. Wright, A. Y. Yang, A. Ganesh, S. S. Sastry, and Y. Ma, "Robust face recognition via sparse representation," *IEEE transactions on pattern analysis and machine intelligence*, vol. 31, no. 2, pp. 210–227, 2009.

[25] W. Xu, Y. Zhang, N. Bergmann, and W. Hu, "Gait-watch: A context-aware authentication system for smart watch based on gait recognition," in *The 2nd ACM/IEEE International Conference on Internet-of-Things Design and Implementation (IOTDI 2017)*. ACM/IEEE, 2017.

[26] Y. Ren, Y. Chen, M. C. Chuah, and J. Yang, "Smartphone based user verification leveraging gait recognition for mobile healthcare systems," in *Sensor, Mesh and Ad Hoc Communications and Networks (SECON), 2013 10th Annual IEEE Communications Society Conference on*. IEEE, 2013, pp. 149–157.

[27] H. Lu, J. Huang, T. Saha, and L. Nachman, "Unobtrusive gait verification for mobile phones," in *Proceedings of the 2014 ACM international symposium on wearable computers*. ACM, 2014, pp. 91–98.

[28] B. Wei, M. Yang, Y. Shen, R. Rana, C. T. Chou, and W. Hu, "Real-time classification via sparse representation in acoustic sensor networks," in *Proceedings of SenSys*. ACM, 2013, p. 21.

[29] Y. Shen, W. Hu, M. Yang, B. Wei, S. Lucey, and C. T. Chou, "Face recognition on smartphones via optimised sparse representation classification," in *Proceedings of IPSN*. IEEE, 2014, pp. 237–248.

[30] Y. Zhang, G. Pan, K. Jia, M. Lu, Y. Wang, and Z. Wu, "Accelerometer-based gait recognition by sparse representation of signature points with clusters," *IEEE transactions on cybernetics*, vol. 45, no. 9, pp. 1864–1875, 2015.

[31] "Design and development of a low cost ubiquitous tracking system," *Procedia Computer Science*, vol. 34, pp. 220 – 227, 2014.

[32] C. Dagdeviren, Z. Li, and Z. L. Wang, "Energy harvesting from the animal/human body for self-powered electronics," *Annual Review of Biomedical Engineering*, vol. 19, no. 1, 2017.

[33] J. Yun, S. Patel, M. Reynolds, and G. Abowd, "A quantitative investigation of inertial power harvesting for human-powered devices," in *Proceedings of the 10th International Conference on Ubiquitous Computing*, ser. UbiComp '08. New York, NY, USA: ACM, 2008, pp. 74–83.

[34] J. Zhao and Z. You, "A shoe-embedded piezoelectric energy harvester for wearable sensors," *Sensors*, vol. 14, no. 7, pp. 12 497–12 510, 2014.

[35] S. J. Hwang, H. J. Jung, J. H. Kim, J. H. Ahn, D. Song, Y. Song, H. L. Lee, S. P. Moon, H. Park, and T. H. Sung, "Designing and manufacturing a piezoelectric tile for harvesting energy from footsteps," *Current Applied Physics*, vol. 15, no. 6, pp. 669–674, 2015.

[36] N. S. Shenck and J. A. Paradiso, "Energy scavenging with shoe-mounted piezoelectrics," *IEEE micro*, vol. 21, no. 3, pp. 30–42, 2001.

[37] G. Lan, D. Ma, W. Xu, M. Hassan, and W. Hu, "Capsense: Capacitor-based activity sensing for kinetic energy harvesting powered wearable devices," in *Proceedings of MobiQuitous*. EAI, 2017.

[38] S. DeBruin, B. Campbell, and P. Dutta, "Monjolo: An energy-harvesting energy meter architecture," in *Proceedings of the 11th ACM Conference on Embedded Networked Sensor Systems*. ACM, 2013, p. 18.

[39] Y. Wang and D. J. Inman, "Simultaneous energy harvesting and gust alleviation for a multifunctional composite wing spar using reduced energy control via piezoceramics," *Journal of Composite Materials*, vol. 47, no. 1, pp. 125–146, 2013.

[40] A. A. Nasir, X. Zhou, S. Durrani, and R. A. Kennedy, "Relaying protocols for wireless energy harvesting and information processing," *IEEE Transactions on Wireless Communications*, vol. 12, no. 7, pp. 3622–3636, 2013.

[41] R. Zhang and C. K. Ho, "Mimo broadcasting for simultaneous wireless information and power transfer," *IEEE Transactions on Wireless Communications*, vol. 12, no. 5, pp. 1989–2001, 2013.

[42] X. Lu, P. Wang, D. Niyato, D. I. Kim, and Z. Han, "Wireless networks with rf energy harvesting: A contemporary survey," *IEEE Communications Surveys & Tutorials*, vol. 17, no. 2, pp. 757–789, 2015.

[43] Y. Dong, M. J. Hossain, and J. Cheng, "Joint power control and time switching for swipt systems with heterogeneous qos requirements," *IEEE Communications Letters*, vol. 20, no. 2, pp. 328–331, 2016.

[44] Q. Shi, L. Liu, W. Xu, and R. Zhang, "Joint transmit beamforming and receive power splitting for miso swipt systems," *IEEE Transactions on Wireless Communications*, vol. 13, no. 6, pp. 3269–3280, 2014.

[45] X. Zhou, R. Zhang, and C. K. Ho, "Wireless information and power transfer: Architecture design and rate-energy tradeoff," *IEEE Transactions on Communications*, vol. 61, no. 11, pp. 4754–4767, 2013.